Russian Journal of Earth Sciences

Spatial Variability of the Hydrochemical Structure in Bottom Gravity Current in the Vema Fracture Zone

O. A. Zuev[1,*], and A. M. Seliverstova[1]

[1] Shirshov Institute of Oceanology, Russian Academy of Sciences, Moscow, Russia
* **Correspondence to:** Oleg A. Zuev, qillous@gmail.com

Abstract: The Vema Fracture Zone is located in the North Atlantic Ridge and extends along 11°N from 38 to 46°W. It is the main pathway for the spreading of Antarctic Bottom Water to the Northeast Atlantic. Due to its location and structure, the Vema Fracture Zone is an excellent object for studying the properties of the bottom gravity flow. An oceanographic section along the entire Vema Fracture Zone was carried out during cruise 52 of the R/V "Akademik Boris Petrov" in November–December 2022. In our work, we analyzed 25 oceanographic stations; at 15 stations, dissolved oxygen and nutrients were also determined. Such studies of the structure of the bottom gravity flow of Antarctic Bottom Water in the central channel of the Vema Fracture Zone based on high spatial resolution in situ data were made for the first time. A supercritical flow accompanied by a hydraulic jump was detected behind the main sill of the fracture zone. Simultaneous measurements of dissolved oxygen, silicate, and phosphate allowed us to examine the hydrochemical structure along the entire Vema Fracture Zone. Its analysis revealed high correlation between the distribution of hydrochemical and oceanographic parameters in both the stable flow and turbulent regimes of the current.

Keywords: bottom gravity current, dissolved oxygen, silicate, hydraulic jump, Antarctic Bottom Water, Vema Fracture Zone.

Citation: Zuev, O. A., and A. M. Seliverstova (2024), Spatial Variability of the Hydrochemical Structure in Bottom Gravity Current in the Vema Fracture Zone, *Russian Journal of Earth Sciences*, 24, ES5002, EDN: DVLXHJ, https://doi.org/10.2205/2024es000945

Introduction

The study of bottom gravity currents has recently received much attention for a long time. Many theoretical and laboratory experiments [*Chesnokov et al.*, 2022; *Hacker and Linden*, 2002; *Lawrence*, 1993; *Lawrence and Armi*, 2022; *Liapidevskii*, 2004; *Whitehead*, 1989; *Zatsepin et al.*, 2005] have been carried out in order to clarify the nature of this phenomenon. There are relatively few works confirming theoretical assumptions in practice [*Hall et al.*, 1997; *Morozov et al.*, 2021; *Simpson*, 1999; *Wesson and Gregg*, 1994] due to the difficulty of obtaining high-quality in situ data. On the one hand, bottom gravity currents weakly interact with the overlying layers and retain their properties at a distance of thousands of kilometers. On the other hand, their ability to transport small particles, stability of their spreading, and the volumes of transported water masses strongly influence the local processes in individual seas [*Emel'yanov et al.*, 2004; *Hansen et al.*, 2001; *Slagstad and McClimans*, 2005] and on the entire World Ocean [*Broecker*, 2010; *Whitehead and Worthington*, 1982]. In addition to the direct influence on the formation of ocean water masses, the study of bottom currents is important for various multidisciplinary aspects, including the study of sedimentation processes [*Glazkova et al.*, 2022], bottom erosion [*Frey et al.*, 2022], the ecology of bottom communities [*Galkin et al.*, 2021], the transfer of

Research Article

Received: 20 August 2024
Accepted: 22 October 2024
Published: 6 November 2024

nutrients [*Holfort and Siedler*, 2001]; this research is also important for the study of many geological, biological and hydrochemical processes. Individual elements such as dissolved oxygen and silicate are classic tracers of water masses [*Krechik et al.*, 2023; *Mantyla and Reid*, 1983; *Orsi et al.*, 1999], while their ability to reflect local oceanographic processes has been poorly studied. The small amount of in situ data with high spatial resolution complicates this task, but can clarify problems in the modern understanding of the dynamics of bottom gravity currents.

This work is devoted to the study of oceanographic and hydrochemical parameters and their spatial variability in the bottom current of Antarctic Bottom Water (AABW) passing through the Vema Fracture Zone (Vema FZ). This deep-water fracture zone is located in the North Atlantic Ridge at 11°N, connects the western and eastern parts of the North Atlantic (Figure 1). It was discovered in 1956 [*Heezen et al.*, 1964]. The Vema FZ is the main pathway for the propagation of AABW first into the Cape Verde Basin and then into the wide basins of the Northeast Atlantic [*Mantyla and Reid*, 1983; *McCartney et al.*, 1991]. Its length exceeds 800 km, the width varies from 8 to 20 km, the maximum depth is more than 5400 m, and the height of the walls above the bottom is 700–900 m [*Vangriesheim*, 1980]. At present, much better data on the Vema FZ relief have become available, in particular multibeam echosounder measurements, which are clearly visible in the latest versions of GEBCO. At the same time, the main features of the relief correspond to those described in [*Vangriesheim*, 1980]. Recent studies show the presence of contourites in the eastern part of the Vema Fracture Zone, which are formed by bottom currents and influence its bottom morphology [*Borisov et al.*, 2023]. Early studies [*Eittreim et al.*, 1983; *Vangriesheim*, 1980] did not find significant velocities of the AABW flow in the Vema Fracture Zone, but subsequent measurements [*Fischer et al.*, 1996; *Morozov et al.*, 2021] confirmed the estimates of velocities of more than 20 cm/s [*McCartney et al.*, 1991]. It should be noted that significant variability of such abyssal flows is observed at tidal and inertial [*Zenk and Visbeck*, 2013], synoptic [*Frey et al.*, 2023; *Liao et al.*, 2016], and multidecadal [*Campos et al.*, 2021; *Zenk and Morozov*, 2007] time scales. The structure of the bottom current in the Vema FZ was also studied based on a three-dimensional ocean circulation model [*Frey et al.*, 2018, 2019], which confirmed the stability of the AABW flow in it. However, direct measurements of hydrochemical parameters in the Vema FZ were absent and were first carried out during the 2022 expedition [*Morozov et al.*, 2023], which allowed us to study their distribution in the bottom gravity current of AABW.

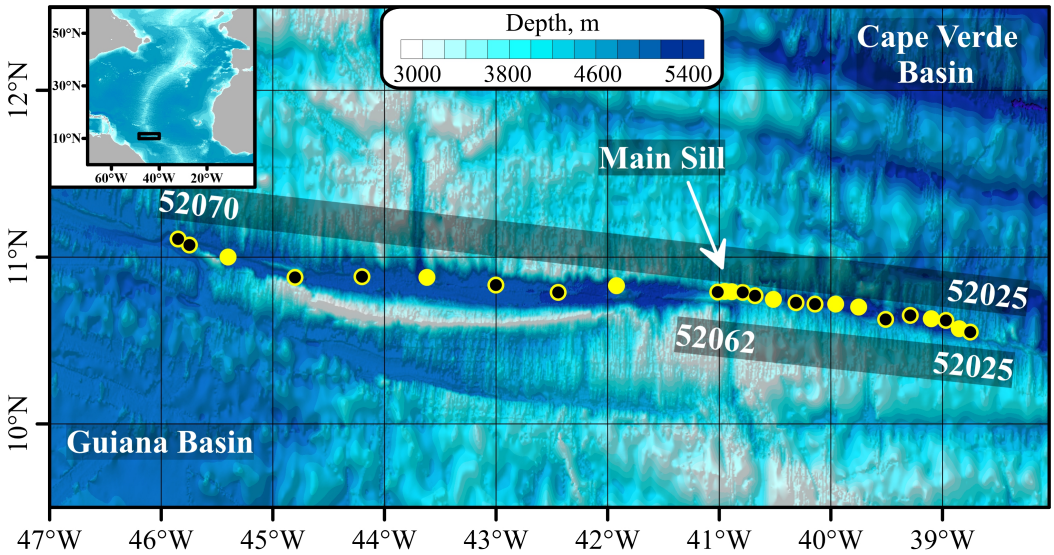

Figure 1. Map of the study site. Dots indicate stations: with oceanographic measurements (yellow), with oceanographic and hydrochemical measurements (yellow-black). The first and last numbers of stations in sections are shown. The bottom relief is shown according to [*GEBCO Bathymetric Compilation Group 2023*, 2023].

Data and Methods

In total, we analyzed 25 oceanographic stations in the central channel of the Vema FZ, at 15 of which hydrochemical indicators were also determined. The locations of the stations and the relief of the Vema FZ are shown (Figure 1).

Oceanographic measurements at stations were made with an Idronaut OCEAN SEVEN 320Plus CTD probe (Italy). The lowered probe is equipped with a high-precision temperature-compensated pressure sensor (PA–10X) with an accuracy of 0.01% and a resolution of 0.002% for the entire measurement range (0–100 MPa), two redundant temperature sensors with a measurement range from –5 to 45 °C, initial accuracy of 0.001 °C, and a resolution of 0.0001 °C. The two redundant conductivity sensors have a measurement range of 0 to 7 S/m, initial accuracy of 0.0001 S/m, and resolution 0.00001 S/m.

The currents were measured with a TRDI Workhorse Monitor Lowered Acoustic Doppler Current profiler (LADCP) with a frequency of 300 kHz. The LADCP data were processed using LDEO Software [*Visbeck*, 2002]. The final measurement accuracy was 3–4 cm/s, for the bottom layers up to 1–2 cm/s owing to bottom track data [*Tarakanov et al.*, 2020]. Additionally, tidal forces calculated using the software described in [*Egbert and Erofeeva*, 2002] were taken into account.

Samples for hydrochemical analyses were taken at the stations with plastic 5-L Niskin bottles of a Carousel Water Sampler system at levels selected based on the vertical potential temperature distribution. Sampling and determination of hydrochemical parameters were carried out in accordance with accepted methods [*Grasshoff et al.*, 1999; *Hansen and Koroleff*, 1999] no later than 6–12 h after sampling.

Results

A detailed analysis of the oceanographic characteristics of the AABW flow along the entire Vema FZ is given in [*Morozov et al.*, 2023], here we will present only the main results that are necessary for further discussion. The main feature of the Vema FZ is its bathymetry – an almost smooth bottom in its western part and very rugged in the area of the main sill at 41°W and to the east largely determines the behavior of the AABW flow. As can be seen from Figure 2, the distributions of oceanographic and hydrochemical parameters differ significantly before and after the main sill of the fracture zone. In the western part, there is a lower stagnant zone with current velocities close to zero and an almost constant potential temperature. This zone occupies about 500 lower meters, and the main flow is located above it – at depths of 3800–4600 m, the velocities here are 10–20 cm/s. However, upon reaching the main sill, the flow accelerates sharply and deepens, which contributes to significant mixing of water and, as a result, its warming. At the same time, the coldest part of the flow cannot overflow the sill at all. This layer differs both in potential temperature and in most hydrochemical indicators. The lowest potential temperature (below 1.4 °C) and dissolved oxygen (less than 5.7 mL/L), the highest phosphate (more than 1.6 μM) and silicate (more than 60 μM) are noted here and are absent beyond the main sill. In turn, in the eastern part of the Vema FZ, a strong deepening of the flow is observed. Accelerating above the main sill, the flow reaches maximum velocities of more than 40 cm/s at the greatest bottom slope near 40.3°W. One result of such strong flow is a warming of water by more than 0.15 °C per 100 km of rough bottom near the main sill of the fracture zone. By the end of the eastern part, the bottom temperature warms by another 0.1 °C and reaches 1.6 °C. This process is also clearly seen in the hydrochemical indicators: in the eastern part of the Vema FZ, the silicate and phosphate at the bottom correspond to the values in the western part at depths of about 4000–4500 m. The most interesting is the distribution of dissolved oxygen; by the end of the section, its values are within the range of 5.75–5.85 mL/L in the entire AABW layer, while at the entrance to the Vema FZ the range of values is much wider – 5.45–5.95 mL/L.

As mentioned earlier, near the main transversal sill of the fracture zone the flow velocity increases significantly. In addition, the vertical gradients of potential temperature and, as a consequence, density increase. At stations 52004–52020, a local thermocline

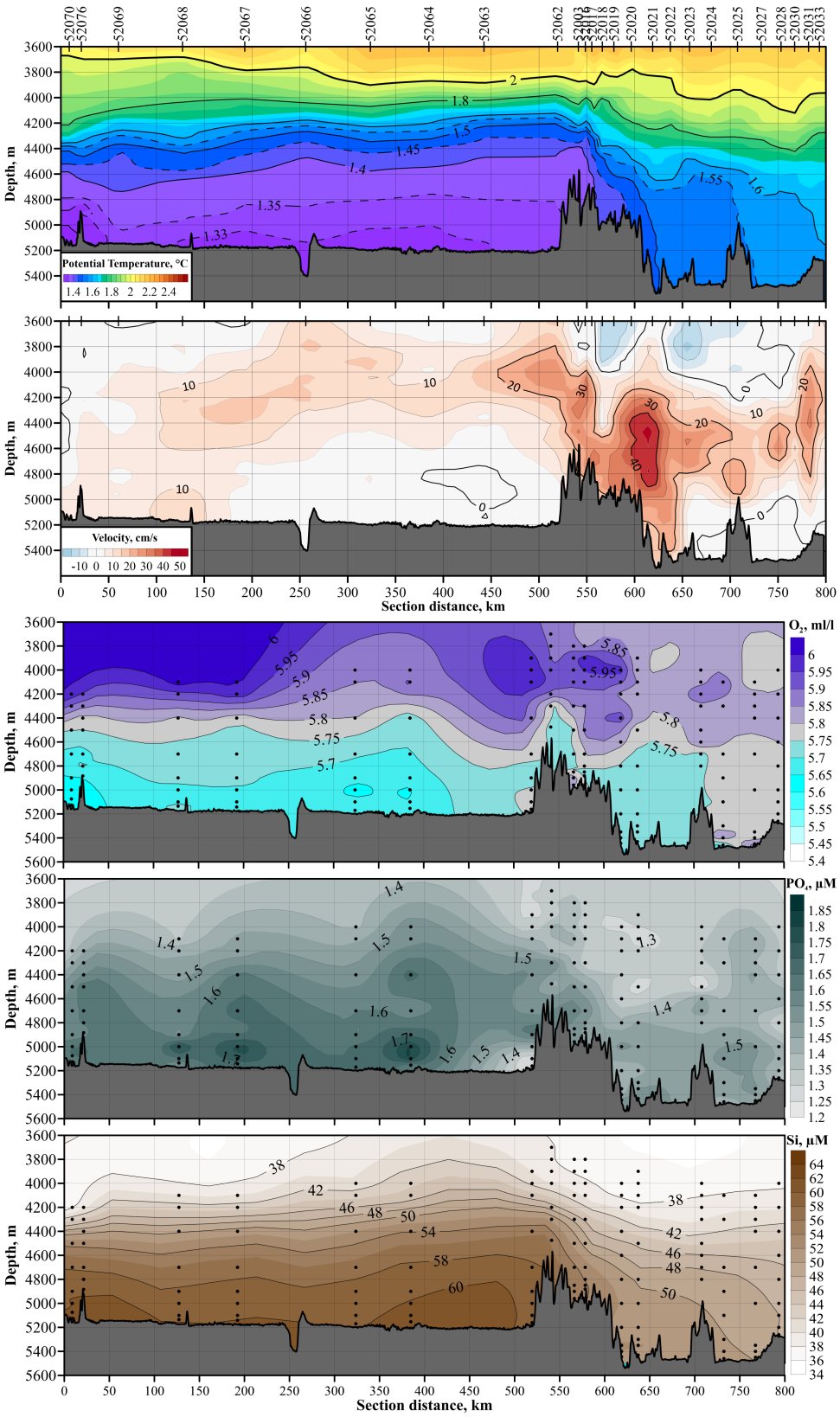

Figure 2. Distribution of potential temperature, LADCP zonal velocity component (positive velocities correspond to the eastern direction), dissolved oxygen, phosphate and silicate over the section along the Vema FZ. The bottom relief is shown according to [*GEBCO Bathymetric Compilation Group 2023*, 2023].

(pycnocline) is observed, which is located in the depth range of 4100–4500 m depending on the station (Figure 3). In addition, other heterogeneities in the stratification of the bottom layer are present in this area, but they are less pronounced. This thermocline also agrees well with the vertical gradients of the flow velocity at most stations. Taking into account that the layers below and above the thermocline are almost homogeneous, we can calculate the steady-state flow regime within the framework of a two-layer model [*Liapidevskii*, 2004; *Pratt and Whitehead*, 2008]. The Froude numbers for the lower layer with a thickness of about 500 m (Table 1) indicate a transition from a subcritical to a supercritical flow at station 52020. Less dense water cannot overcome the thermocline and continues to move in the 4400–4800 m layer in the form of an intrusion. In this case, the intrusion flow and its continuation are present throughout the eastern part of the fracture zone, and the bottom flow is observed only at the station next to the slope; then its energy dissipates and it stops. The isotherms behave accordingly: at the slope stations, they descend to a depth of about 150 m; then, they return to the initial depth. The so-called hydraulic jump occurs with a sharp deepening of denser waters; it can contribute to the strengthening of internal waves and is one of the signs of an underwater spillway. Similar effects and Froude number values have been observed in some other deep channels [*Pratt and Whitehead*, 2008; *Tarakanov et al.*, 2018; *Wesson and Gregg*, 1994], and most often occur with a sharp change in the ocean depth.

Table 1. Froude number at each station is calculated as $Fr = v/\sqrt{g'H}$, where v is the average velocity of bottom flow, g' is the reduced acceleration due to gravity, H is the characteristic scale of bottom layer.

Station	52004	52016	52017	52018	52019	52020	52021	52022
v, m/s	0.36	0.25	0.27	0.26	0.29	0.35	0.22	0.25
g', m/s^2	0.00031	0.00021	0.00022	0.00016	0.00025	0.00011	0.00012	0.00011
H, m	550	460	400	500	500	500	600	680
Fr	0.87	0.81	0.91	0.91	0.82	1.49	0.80	0.92

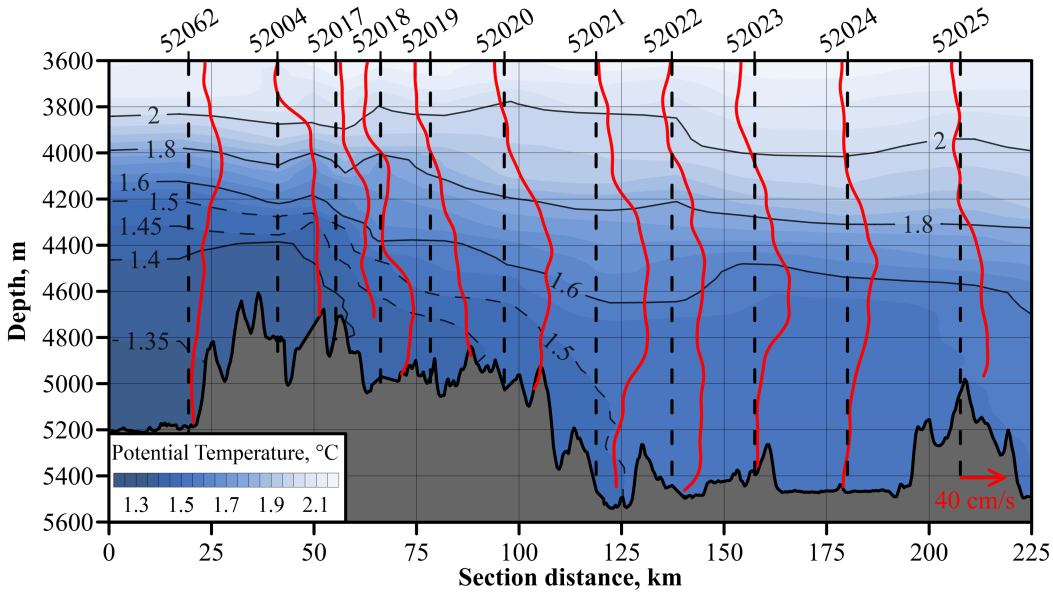

Figure 3. Distribution of potential temperature and LADCP zonal velocity component (red lines) over eastern part of the Vema FZ. The bottom relief is shown according to [*GEBCO Bathymetric Compilation Group 2023*, 2023].

It was interesting to follow the changes in the hydrochemical parameters in such a dynamic water flow. Let us consider individual graphs of dissolved oxygen and silicate in comparison with the potential temperature and current velocity (Figure 4). It is easy to see the similarity in the distribution of dissolved oxygen and silicate with the potential temperature almost throughout the entire depth. The largest vertical gradients of dissolved oxygen and silicate fall on the local thermocline, and below it the distribution is homogeneous – 5.7–5.75 mL/L and 50–55 μM, respectively. At the stations after the slope, the concentration of dissolved oxygen slightly increases, and silicate decreases, as do the potential temperatures. This is how the entrainment of water from the thermocline is manifested during the hydraulic jump. However, the hydrochemical parameters in the lower 500 m layer are homogeneous throughout the entire depth, which indicates the duration of the mixing processes and, probably, the constancy of the observed dynamic structure in a given location. The graph of dissolved oxygen at station 52022 stands out: its distribution becomes uniform even at depths shallower than 4500 m, the spread of values is only 0.15 mL/L, compared to 0.30 mL/L at the previous station.

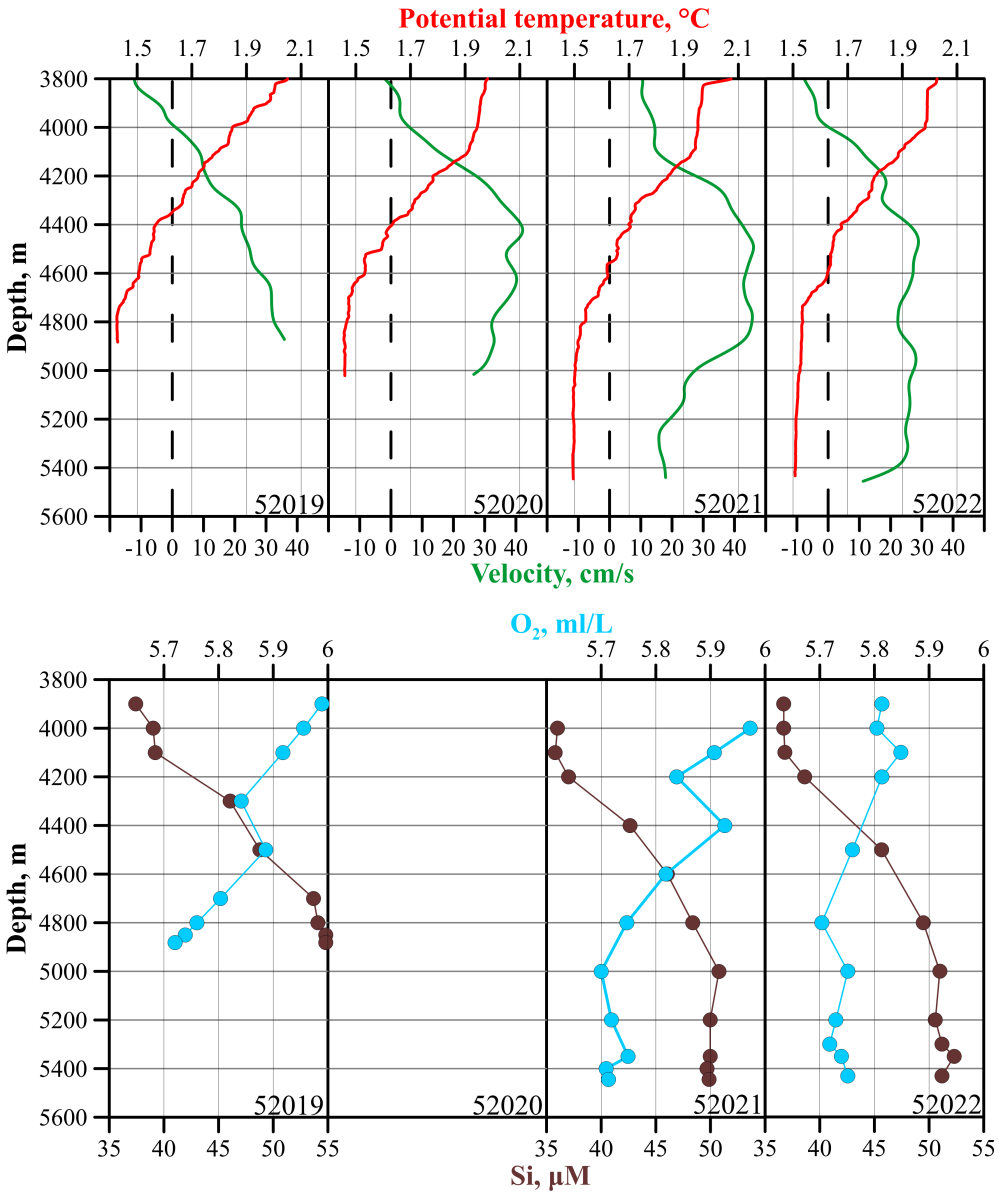

Figure 4. Distributions of potential temperature (red), LADCP zonal component of velocity (green), dissolved oxygen (blue) and silicate (brown) at the stations on the slope. Hydrochemical measurements were not carried out at station 52020.

Conclusions

A strong flow of AABW is observed in the Vema FZ. West of the main sill at 41°W the flow accelerates in the layer close to 4000 m. Below this depth there is a stagnation zone in front of the sill. Strong spillway is observed downslope of the main sill with Froude numbers exceeding unity, which makes the flow supercritical. Correlation between the distribution of hydrological and hydrochemical parameters is observed throughout the entire Vema FZ. The distribution of dissolved oxygen, phosphate and silicate corresponds to the thermohaline structure and dynamics of the waters. This is manifested both in the layer with low bottom current velocities and in the zone with a supercritical regime and strong mixing. This fact indicates the stability of the observed dynamic structure in the Vema FZ.

Acknowledgements. This study was supported by the Russian Science Foundation, grant 24-27-00181.

References

Borisov, D. G., D. I. Frey, E. V. Ivanova, et al. (2023), Unveiling the contourite depositional system in the Vema Fracture Zone (Central Atlantic), *Scientific Reports*, *13*(1), https://doi.org/10.1038/s41598-023-40401-4.

Broecker, W. (2010), *The Great Ocean Conveyor: Discovering the Trigger for Abrupt Climate Change*, Princeton University Press, https://doi.org/10.1515/9781400834716.

Campos, E. J. D., van M. C. Caspel, W. Zenk, et al. (2021), Warming Trend in Antarctic Bottom Water in the Vema Channel in the South Atlantic, *Geophysical Research Letters*, *48*(19), https://doi.org/10.1029/2021GL094709.

Chesnokov, A. A., S. L. Gavrilyuk, and V. Y. Liapidevskii (2022), Mixing and nonlinear internal waves in a shallow flow of a three-layer stratified fluid, *Physics of Fluids*, *34*(7), https://doi.org/10.1063/5.0093754.

Egbert, G. D., and S. Y. Erofeeva (2002), Efficient Inverse Modeling of Barotropic Ocean Tides, *Journal of Atmospheric and Oceanic Technology*, *19*(2), 183–204, https://doi.org/10.1175/1520-0426(2002)019<0183:eimobo>2.0.co;2.

Eittreim, S. L., P. E. Biscaye, and S. S. Jacobs (1983), Bottom-water observations in the Vema fracture zone, *Journal of Geophysical Research: Oceans*, *88*(C4), 2609–2614, https://doi.org/10.1029/JC088iC04p02609.

Emel'yanov, E. M., V. A. Gritsenko, and V. D. Egorikhin (2004), Near-bottom circulation in the gdansk deep of the baltic sea: Bottom sediments and dynamcis of inflows of the north sea waters, *Oceanology*, *44*(2), 261–273, EDN: LILRZH.

Fischer, J., M. Rhein, F. Schott, and L. Stramma (1996), Deep water masses and transports in the Vema Fracture Zone, *Deep Sea Research Part I: Oceanographic Research Papers*, *43*(7), 1067–1074, https://doi.org/10.1016/0967-0637(96)00044-1.

Frey, D., D. Borisov, V. Fomin, E. Morozov, and O. Levchenko (2022), Modeling of bottom currents for estimating their erosional-depositional potential in the Southwest Atlantic, *Journal of Marine Systems*, *230*, 103,736, https://doi.org/10.1016/j.jmarsys.2022.103736.

Frey, D. I., E. G. Morozov, V. V. Fomin, and N. A. Diansky (2018), Spatial Structure of the Antarctic Water Flow in the Vema Fracture Zone of the Mid-Atlantic Ridge, *Izvestiya, Atmospheric and Oceanic Physics*, *54*(6), 621–625, https://doi.org/10.1134/S0001433818060063.

Frey, D. I., E. G. Morozov, V. V. Fomin, N. A. Diansky, and R. Y. Tarakanov (2019), Regional Modeling of Antarctic Bottom Water Flows in the Key Passages of the Atlantic, *Journal of Geophysical Research: Oceans*, *124*(11), 8414–8428, https://doi.org/10.1029/2019JC015315.

Frey, D. I., E. G. Morozov, and D. A. Smirnova (2023), Sea level anomalies affect the ocean circulation at abyssal depths, *Scientific Reports*, *13*(1), https://doi.org/10.1038/s41598-023-48074-9.

Galkin, S. V., K. V. Minin, A. A. Udalov, et al. (2021), Benthic Assemblages of the Powell Basin, *Oceanology*, *61*(2), 204–219, https://doi.org/10.1134/S0001437021020053.

GEBCO Bathymetric Compilation Group 2023 (2023), The GEBCO_2023 Grid - a continuous terrain model of the global oceans and land, https://doi.org/10.5285/F98B053B-0CBC-6C23-E053-6C86ABC0AF7B.

Glazkova, T., F. J. Hernández-Molina, E. Dorokhova, et al. (2022), Sedimentary processes in the Discovery Gap (Central-NE Atlantic): An example of a deep marine gateway, *Deep Sea Research Part I: Oceanographic Research Papers*, *180*, 103,681, https://doi.org/10.1016/j.dsr.2021.103681.

Grasshoff, K., K. Kremling, and M. Ehrhardt (Eds.) (1999), *Methods of Seawater Analysis*, Wiley, Hoboken, https://doi.org/10.1002/9783527613984.

Hacker, J. N., and P. F. Linden (2002), Gravity currents in rotating channels. Part 1. Steady-state theory, *Journal of Fluid Mechanics*, *457*, 295–324, https://doi.org/10.1017/S0022112001007662.

Hall, M. M., M. McCartney, and J. A. Whitehead (1997), Antarctic Bottom Water Flux in the Equatorial Western Atlantic, *Journal of Physical Oceanography*, *27*(9), 1903–1926, https://doi.org/10.1175/1520-0485(1997)027<1903:ABWFIT>2.0.CO;2.

Hansen, B., W. R. Turrell, and S. Østerhus (2001), Decreasing overflow from the Nordic seas into the Atlantic Ocean through the Faroe Bank channel since 1950, *Nature*, *411*(6840), 927–930, https://doi.org/10.1038/35082034.

Hansen, H. P., and F. Koroleff (1999), Determination of nutrients, in *Methods of Seawater Analysis*, pp. 159–228, Wiley, https://doi.org/10.1002/9783527613984.ch10.

Heezen, B. C., R. D. Gerard, and M. Tharp (1964), The Vema fracture zone in the equatorial Atlantic, *Journal of Geophysical Research*, *69*(4), 733–739, https://doi.org/10.1029/JZ069i004p00733.

Holfort, J., and G. Siedler (2001), The Meridional Oceanic Transports of Heat and Nutrients in the South Atlantic, *Journal of Physical Oceanography*, *31*(1), 5–29, https://doi.org/10.1175/1520-0485(2001)031<0005:TMOTOH>2.0.CO;2.

Krechik, V. A., M. V. Kapustina, D. I. Frey, et al. (2023), Properties of Antarctic Bottom Water in the Western Gap (Azores-Gibraltar Fracture Zone, Northeast Atlantic) in 2021, *Deep Sea Research Part I: Oceanographic Research Papers*, *202*, 104,191, https://doi.org/10.1016/j.dsr.2023.104191.

Lawrence, G. A. (1993), The hydraulics of steady two-layer flow over a fixed obstacle, *Journal of Fluid Mechanics*, *254*, 605–633, https://doi.org/10.1017/S0022112093002277.

Lawrence, G. A., and L. Armi (2022), Stationary internal hydraulic jumps, *Journal of Fluid Mechanics*, *936*, https://doi.org/10.1017/jfm.2022.74.

Liao, G., B. Zhou, C. Liang, et al. (2016), Moored observation of abyssal flow and temperature near a hydrothermal vent on the Southwest Indian Ridge, *Journal of Geophysical Research: Oceans*, *121*(1), 836–860, https://doi.org/10.1002/2015JC011053.

Liapidevskii, V. Y. (2004), Mixing Layer on the Lee Side of an Obstacle, *Journal of Applied Mechanics and Technical Physics*, *45*(2), 199–203, https://doi.org/10.1023/B:JAMT.0000017582.70655.d9.

Mantyla, A. W., and J. L. Reid (1983), Abyssal characteristics of the World Ocean waters, *Deep Sea Research Part A. Oceanographic Research Papers*, *30*(8), 805–833, https://doi.org/10.1016/0198-0149(83)90002-X.

McCartney, M. S., S. L. Bennett, and M. E. Woodgate-Jones (1991), Eastward Flow through the Mid-Atlantic Ridge at 11°N and Its Influence on the Abyss of the Eastern Basin, *Journal of Physical Oceanography*, *21*(8), 1089–1121, https://doi.org/10.1175/1520-0485(1991)021<1089:EFTTMA>2.0.CO;2.

Morozov, E. G., R. Y. Tarakanov, and D. I. Frey (2021), *Bottom Gravity Currents and Overflows in Deep Channels of the Atlantic Ocean: Observations, Analysis, and Modeling*, Springer International Publishing, https://doi.org/10.1007/978-3-030-83074-8.

Morozov, E. G., D. I. Frey, O. A. Zuev, et al. (2023), Antarctic Bottom Water in the Vema Fracture Zone, *Journal of Geophysical Research: Oceans*, *128*(8), https://doi.org/10.1029/2023JC019967.

Orsi, A. H., G. C. Johnson, and J. L. Bullister (1999), Circulation, mixing, and production of Antarctic Bottom Water, *Progress in Oceanography*, *43*(1), 55–109, https://doi.org/10.1016/S0079-6611(99)00004-X.

Pratt, L. J., and J. A. Whitehead (2008), *Rotating Hydraulics: Nonlinear Topographic Effects in the Ocean and Atmosphere*, 36, Springer New York, New York, https://doi.org/10.1007/978-0-387-49572-9.

Simpson, J. E. (1999), *Gravity currents: In the environment and the laboratory*, Cambridge University Press.

Slagstad, D., and T. A. McClimans (2005), Modeling the ecosystem dynamics of the Barents sea including the marginal ice zone: I. Physical and chemical oceanography, *Journal of Marine Systems*, *58*(1–2), 1–18, https://doi.org/10.1016/j.jmarsys.2005.05.005.

Tarakanov, R. Y., E. G. Morozov, H. van Haren, N. I. Makarenko, and T. A. Demidova (2018), Structure of the Deep Spillway in the Western Part of the Romanche Fracture Zone, *Journal of Geophysical Research: Oceans*, *123*(11), 8508–8531, https://doi.org/10.1029/2018JC013961.

Tarakanov, R. Y., E. G. Morozov, and D. I. Frey (2020), Hydraulic Continuation of the Abyssal Flow From the Vema Channel in the Southwestern Part of the Brazil Basin, *Journal of Geophysical Research: Oceans*, *125*(6), https://doi.org/10.1029/2020JC016232.

Vangriesheim, A. (1980), Antarctic Bottom Water flow through the Vema Fracture Zone, *Oceanologica Acta*, *3*(2), 199–207.

Visbeck, M. (2002), Deep Velocity Profiling Using Lowered Acoustic Doppler Current Profilers: Bottom Track and Inverse Solutions, *Journal of Atmospheric and Oceanic Technology*, *19*(5), 794–807, https://doi.org/10.1175/1520-0426(2002)019<0794:DVPULA>2.0.CO;2.

Wesson, J. C., and M. C. Gregg (1994), Mixing at Camarinal Sill in the Strait of Gibraltar, *Journal of Geophysical Research: Oceans*, *99*(C5), 9847–9878, https://doi.org/10.1029/94JC00256.

Whitehead, J. A. (1989), Internal hydraulic control in rotating fluids-applications to oceans, *Geophysical & Astrophysical Fluid Dynamics*, *48*(1–3), 169–192, https://doi.org/10.1080/03091928908219532.

Whitehead, J. A., and L. V. Worthington (1982), The flux and mixing rates of Antarctic bottom water within the North Atlantic, *Journal of Geophysical Research: Oceans*, *87*(C10), 7903–7924, https://doi.org/10.1029/JC087iC10p07903.

Zatsepin, A. G., V. V. Kremenetskii, S. G. Poyarkov, et al. (2005), Laboratory and numerical study of gravity currents over a sloping bottom, *Oceanology*, *45*(1), 1–10, EDN: LJKEPF.

Zenk, W., and E. Morozov (2007), Decadal warming of the coldest Antarctic Bottom Water flow through the Vema Channel, *Geophysical Research Letters*, *34*(14), https://doi.org/10.1029/2007GL030340.

Zenk, W., and M. Visbeck (2013), Structure and evolution of the abyssal jet in the Vema Channel of the South Atlantic, *Deep Sea Research Part II: Topical Studies in Oceanography*, *85*, 244–260, https://doi.org/10.1016/j.dsr2.2012.07.033.